Electronic Structure, Stability, and Electrical Mobility of Cationic Silver Oxide Atomic Clusters

Bhowmick, Somnath; Maisser, Anne; Suleimanov, Yury V.; Schmidt-Ott, Andreas; Biskos, George

DOI
10.1021/acs.jpca.2c02809

Publication date
2022

Document Version
Final published version

Published in
Journal of Physical Chemistry A

THE JOURNAL OF PHYSICAL CHEMISTRY A
A JOURNAL OF THE AMERICAN CHEMICAL SOCIETY

pubs.acs.org/JPCA

Article

Electronic Structure, Stability, and Electrical Mobility of Cationic Silver Oxide Atomic Clusters

Somnath Bhowmick, Anne Maisser, Yury V. Suleimanov, Andreas Schmidt-Ott, and George Biskos*

Cite This: *J. Phys. Chem. A* 2022, 126, 6376−6386

Read Online

ACCESS | Metrics & More | Article Recommendations | Supporting Information

ABSTRACT: Silver oxide cluster cations ($Ag_nO_m^+$) can readily be produced by a number of methods including atmospheric-pressure spark ablation of pure silver electrodes when trace amounts of oxygen are present in the carrier gas. Here we determine the equilibrium geometries of $Ag_nO_m^+$ clusters (n = 1−4; m = 1−5) using accurate coupled cluster with singles and doubles (CCSD) method, while the stabilization energies are calculated with additional perturbative triples correction (CCSD(T)). Although a number of stable states have been identified, our results show that the $Ag_nO_m^+$ clusters with m = 1 are more stable than those with $m \geq 2$ due to the absence of the terminally attached O_2 molecule, corroborating recent observations by mass spectrometry. Using the computed structures, we calculate the electrical mobilities of the $Ag_nO_m^+$ clusters and label the values on a respective experimentally determined spectrum in an attempt to better interpret the occurrence of the peaks and troughs in the measurements.

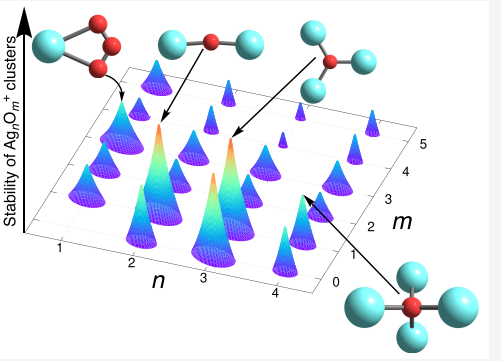

1. INTRODUCTION

Silver is a noble metal that has traditionally been employed in a wide range of applications. For example, ancient Greeks, Romans, and Egyptians used silver for a variety of medical applications[1] and as a food or water preservative.[2] In the form of nanoparticles (i.e., particles having sizes up to ∼100 nm), silver is extensively being employed as an effective antimicrobial agent,[3] as well as in applications including catalysis,[4,5] sensing and imaging,[6,7] as well as for synthesizing new electronic materials,[8] among others. Silver clusters containing up to tens of atoms have further extended the application of this noble metal in optoelectronics,[9] plasmonics,[10] biomedicine,[11] and DNA sequencing.[12]

Considering the high interest in silver clusters, developing synthesis processes with good scalability is highly important. In this respect, spark ablation[13] provides a versatile method for synthesizing metal-based clusters and nanoparticles, having a number of advantages, including good control over the size and composition of the resulting clusters/nanoparticles.[13,14] Typically, spark ablation is operated at atmospheric pressure with carrier gases that unavoidably contain trace amounts of impurities, including oxygen, that can affect the composition of the resulting clusters.

The stable geometries of pure silver clusters, including their ions, are among the most well-established.[13,15−21] For a period, it was believed that silver clusters did not react with O_2.[22] However, experimental evidence showed that they could be oxidized under certain conditions.[15,18,23−31] In light of that, a number of studies have explored the stabilities and geometries of the charged silver oxide clusters.[18,23,27,28,31−34] Schmidt et al.[18] have produced silver oxide clusters (i.e., Ag_nO^+ and $Ag_nO_2^+$ with n = 1−9) and observed that stabilities follow the magic numbers (i.e., shell closing at 2, 8, 20, 40, 58, etc., free electrons), whereas the most favored dissociation channel is the elimination of a silver monomer or dimer. They have also determined the minimum energy structures of these oxidized clusters by *ab initio* density functional theory (DFT) calculations using Perdew, Burk, and Ernzerhof (PBE) generalized gradient approximation (GGA) functionals[35] with a plane-wave basis function. In contrast to Ag_n^+ clusters with $n \leq 7$, their oxidized products Ag_nO^+ and $Ag_nO_2^+$ adopt a 3D structure even for values of n as small as 3. Wang and Gong[34] also determined the minimum energy structures and stabilities of $Ag_nO_m^+$ (n = 1−6, m = 1−2) clusters by the local spin density approximation (LSDA)[36] method using projector augmented-wave (PAW)[37] potentials. In general, their calculations corroborate those reported by Schmidt et al.[18]

The results of Schmidt et al. and Wang et al. are in contrast to independent calculations reported by Roithová et al.[33] and Flurer et al.[23] In the case of Ag_2O^+, for example, Roithová and co-worker[33] found the ground-state geometry to be almost linear (∠AgOAg = 179.8°), whereas Schmidt et al.[18] and Wang et al.[34] reported a triangular geometry with ∠AgOAg = 149.0° and 138.1°, respectively. Flurer and co-workers[23] also

Received: April 22, 2022
Revised: August 31, 2022
Published: September 13, 2022

determined a linear geometry, albeit using a less accurate Hartree−Fock (HF) self-consistent field (SCF) level of theory. Wang et al. found that the linear geometry is less stable and lies at least 0.03 eV above the energy of triangular geometry. It is interesting to note that the calculations reported in the literature so far have been performed within the HF or DFT formalism. As a result, and considering the contradicting calculations reported so far, it is of utmost importance to re-evaluate the ground-state geometries of the $Ag_nO_m^+$ clusters with a more sophisticated electronic structure theory.

In addition to the information provided by electronic structure theory, determining the electrical mobility of the ionic clusters both theoretically and experimentally is highly useful for gaining insights into their size and morphology. The electrical mobility (a measure of drift velocity) at a particular pressure and temperature is inversely proportional to the average collision cross-section (CCS; a measure of size).[38,39] Jarrold and co-workers[40,41] have shown that the CCS can be calculated through quantum chemical considerations. Naturally, the accuracy of the calculated CCS depends on the geometry of the clusters, which can be determined by *ab initio* calculations, and consequently on the specific method employed. For the pure silver cluster cations (Ag_n^+, $n < 12$), Weis et al.[17] found that both experimentally measured and theoretically determined CCS values are in good agreement with each other, although significant discrepancies were reported for some other cases. More recently, Maisser et al. determined the electrical mobilities of both positively and negatively charged silver-based clusters having up to 25 Ag atoms.[13] The clusters were produced by spark ablation, and subsequently, their mobility was determined by a Differential Mobility Analyzer (DMA; ref 42) at atmospheric pressure. As stated, considering that carrier gases, even after high purification processing, can contain trace amounts of impurities, including oxygen, the resulting aerosol contains a high fraction of stable oxidized clusters produced by the etching effect.[43] Therefore, it is advantageous to reassign the broad electrical mobility spectra obtained for silver cluster cations by also adding their oxidized variants.

In this work, we theoretically determine the minimum energy structure, stabilization energy, and electrical mobility of $Ag_nO_m^+$ clusters. We compare the calculated stabilization energies and the mobilities of the ionic clusters with experimentally determined mass and electrical mobility spectra, respectively. For the electronic energy calculations, we used a very accurate coupled cluster (CC) with single (S), double (D), and perturbative triple (T) excitation (CCSD(T)) level of theory.[44−47] Because the CCSD(T) method scales with the number of basis sets as $O(N^7)$[48] and, consequently, substantial computational costs are associated with very large systems, we have restricted our calculations to clusters with $n = 1−4$ and $m = 1−5$. The rest of the paper is organized in three sections, with section 2 giving details of the computational methods used in this work, section 3 providing a discussion on the stable geometries, dissociation energies, and electrical mobilities of the $Ag_nO_m^+$ clusters, and section 4 highlighting the most important conclusions.

2. COMPUTATIONAL DETAILS

2.1. Electronic Structure Calculations. We have used the Gaussian 16 package,[49] in combination with the isomer module of the ABCluster program,[50−52] to search systematically for the best candidate structures of $Ag_nO_m^+$ clusters with $n = 1−4$ and $m = 1−5$. The ABCluster estimates the potential energy of a configuration and then constitutes a set of the best trial solutions by an efficient feedback-knowledge loop. Full dimensional geometry optimizations have been performed from this pool of structures at the M06[53] level of theory, which has been reported to produce electronic properties that are consistent with experimental observations for the charged silver clusters.[21]

A few of the low energy structures obtained at the M06 level are subsequently optimized at the CCSD level of theory[44−46] with a tighter energy convergence (2×10^{-9} Hartree). Finally, single-point energy calculations on the geometries optimized by the CCSD method have been performed by the more accurate CCSD(T) theory[47] to account for the ground-state electronic energy. For the ground-state wave function that is essentially a single-reference character, the CCSD(T) method is often termed as the "gold standard" of quantum chemistry due to its ability to obtain accurate bond energies and molecular properties of reasonably large molecules.[48] Truhlar et al.[19] showed that the M06 method could accurately predict all low-energy isomers of charged silver clusters, whereas the differences of the relative energy are also in good agreement with the CCSD(T) calculations[54] (below approximately ±0.1 eV). In this study, all isomers found in the M06 method that have energies below 1.0, 0.75, and 0.5 eV in comparison to the lowest energy isomer for $n \leq 2$, 3, and 4, respectively, are taken into consideration for the CCSD calculations. Harmonic frequency analysis has also been performed on all isomers to verify the local minima on the potential energy surface.

In this study, we calculated the two spin states for each cluster: i.e., singlet and triplet state for even numbers and doublet and quartet state for odd numbers of electrons. We have chosen the standard Dunning's augmented correlation-consistent triple-ζ basis set (aug-cc-pVTZ) for the oxygen atoms (contracted to 5s4p3d2f),[55,56] and the cc-pVTZ basis set (contracted to 5s5p4d2f1g) with the inner core electrons described by Stuttgart/Köln energy consistent pseudopotential (ECP28MDF) for the silver atoms.[57,58]

The zero-point vibrational energy (ZPVE) corrected stabilization energy (ΔE) of the clusters were calculated with respect to the lowest energy dissociation channel $Ag_nO_m^+ \rightarrow Ag_{n-x}O_{m-y}^+ + Ag_xO_y$ (i.e., the unimolecular dissociative reaction of the $Ag_nO_m^+$ clusters absorbing least/releasing most energy) as[18,34]

$$\Delta E = E(Ag_{n-x}O_{m-y}^+) + E(Ag_xO_y) - E(Ag_nO_m^+) \quad (1)$$

where, $E(Ag_{n-x}O_{m-y}^+)$, $E(Ag_xO_y)$, and $E(Ag_nO_m^+)$ are the total energies of $Ag_{n-x}O_{m-y}^+$, Ag_xO_y, and $Ag_nO_m^+$ clusters, respectively. We should note that x and y can take any value from 0 to n and 0 to m, respectively, with the constraint that they cannot be both zero simultaneously.

2.2. Collision Cross-Section and Electrical Mobility Calculation. The CCS and electrical mobility of the lowest energy ionic structures were calculated by the MOBCAL code.[40] The electrical mobility Z of the ions were determined as[40]

$$Z = \frac{(18\pi)^{1/2}}{16}\left[\frac{1}{m} + \frac{1}{m_B}\right]^{1/2}\frac{ze}{(k_BT)^{1/2}\Omega}\frac{1}{N} \quad (2)$$

Here, m and m_B are respectively the mass of the ion and carrier gas atom, z is the number of elementary charge (e) carried by the ion, k_B is the Boltzmann constant, T is the effective temperature, N is the number density of the gas, and Ω is the average CCS, which was calculated here by three different approaches: (i) the projection approximation (PA),[59] (ii) the exact hard-spheres

https://doi.org/10.1021/acs.jpca.2c02809
J. Phys. Chem. A 2022, 126, 6376−6386

scattering (EHSS),[41] and (iii) the trajectory method (TM).[40] The hard-sphere radius r_{hs} and 12−6 Lennard-Jones parameters that are required for the calculation of the CCSs with the three methods mentioned above are provided in Table 1.

Table 1. Hard Sphere Radius (r_{hs}; Å), 12-6 Lennard-Jones Parameters of Energy (ϵ; meV), and Van der Waals Distance (σ; Å) for O and Ag Atoms

		12−6 Lennard-Jones parameters	
species	r_{hs}	ϵ	σ
O	1.52[a]	1.07[b]	2.43[b]
Ag	1.57[c]	1.35[d]	3.00[d]

[a]Ref 60. [b]Ref 61. [c]Ref 17. [d]Ref 62.

It has been reported that, when used for mobility or CCS calculations, the chosen values of the parameters provided in Table 1 show good correspondence with the experimental results.[17,61,62] For example, Weis et al. found excellent agreement with experimental results when either the r_{hs} or the 12−6 Lennard-Jones parameters, as mentioned in Table 1, were used to calculate the CCS of pure cationic silver clusters[17] (Ag_n^+ with $n < 12$) or mixed silver−gold cation clusters[62] ($Ag_mAu_n^+$ with $m + n < 6$), respectively. On the other hand, the ϵ and σ values of O atoms have been optimized by using drift-tube measurements of CCSs for oxygen-containing organic compounds.[61]

We have also performed preliminary calculations of the CCS and Z using the parameters in Table 1 and found good agreement with reported experimental values. For example, the experimental CCS (32.5 Å^2) of Ag_2^+ measured by Weis et al.[17] is very close to the values calculated by the three methods (ranging between 31.8 and 33.1 Å^2). The experimentally determined electrical mobility of the O_2^+ ion (21.8 ± 1.7 cm^2 V^{-1} s^{-1})[63] is also in good agreement with calculated results (22.2−23.3 cm^2 V^{-1} s^{-1}). Furthermore, we have analyzed the sensitivity of the mobility calculations with respect to the chosen values of the parameters and found that, for a 10% change in ϵ and σ, there is a corresponding ∼1% and ∼11% deviation in the CCS values calculated by the TM method, as well as in the corresponding electrical mobilities. In contrast, the same change in the hard-sphere radius (r_{hs}) parameter induces at least 18% deviation in the CCS values predicted by the PA and EHSS approaches.

We run 5×10^7 classical trajectories for each TM simulation, with the charge distribution on each atomic center being determined by the Natural Population Analysis (NPA).[64] We should note here that NPA has been reported to have excellent numerical stability with respect to variations in basis set and method,[65] and good agreement with the empirical structure−function relationship.[66] Since the experimental mobility spectrum has been obtained using helium as the carrier gas,[13] for a direct comparison, the mobility calculations have been performed using the same gas having a polarizability of 0.205 Å^3. We should note that all calculations have been performed at 20 °C and 1 atm pressure.

3. RESULTS AND DISCUSSION

3.1. Electronic Properties of the $Ag_nO_m^+$ Clusters. The ground-state structures of the $Ag_nO_m^+$ clusters are illustrated in Figures 1−4, and the corresponding coordinates are provided in Tables S1−S20. In general, as the size of the clusters increases,

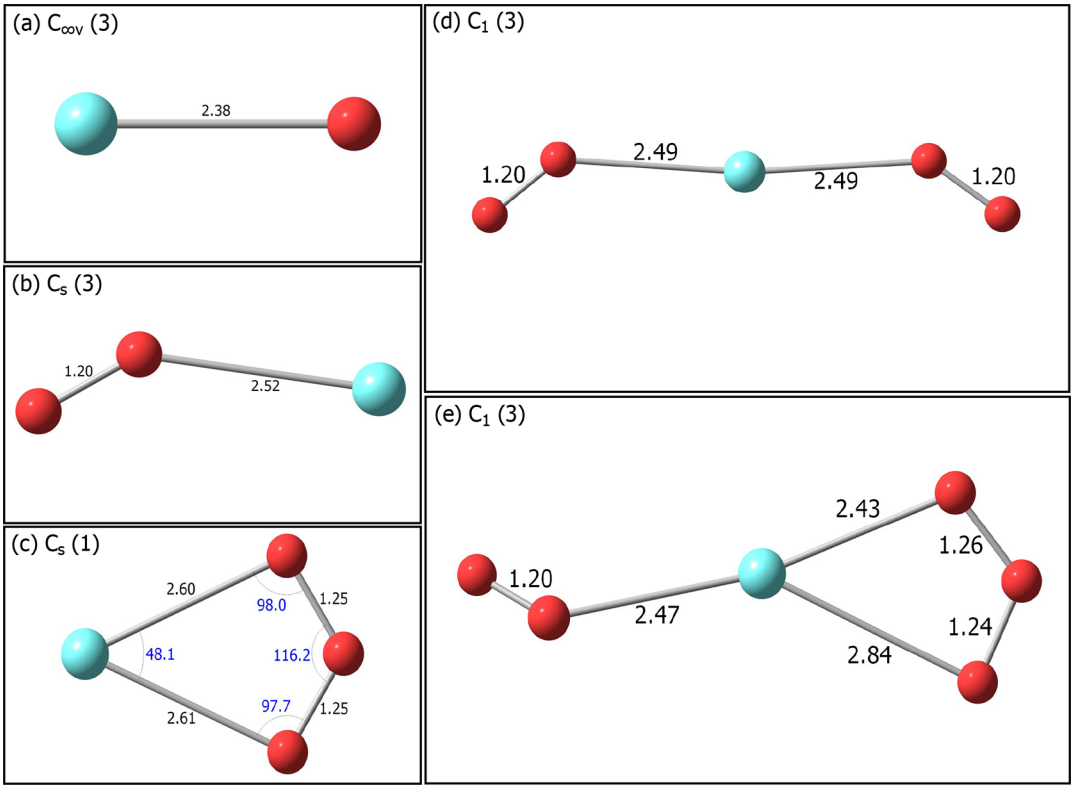

Figure 1. Ground-state structures of the AgO_m^+ clusters, optimized by the CCSD method, where $m = 1−5$. Red spheres denote oxygen atoms, and the cyan sphere indicates the silver atom of the clusters. Bond lengths (black fonts) and angles (blue fonts) are given in ångstroms and degrees, respectively. Spin multiplicities are provided in parentheses.

https://doi.org/10.1021/acs.jpca.2c02809
J. Phys. Chem. A 2022, 126, 6376−6386

Table 2. Summary of the CCSD(T) and Electrical Mobility Calculations on the Ground State of AgO_m^+, $Ag_2O_m^+$, $Ag_3O_m^+$, and $Ag_4O_m^+$ Clusters, Where, m = 1−5[a]

							Ω			Z^{-1}		
species	m	$2S+1$	PG	ΔE	μ	VEA	PA	EHSS	TM	PA	EHSS	TM
AgO_m^+	1	3	$C_{\infty v}$	0.49	1.06	7.19	29.45	29.77	29.59	499.97	505.42	502.33
	2	3	C_s	0.28	2.21	6.85	34.71	35.30	33.50	590.26	600.30	569.72
	3	1	C_s	0.78	1.90	7.43	36.84	37.44	34.34	627.35	637.57	584.84
	4	3	C_1	−0.17	0.33	6.96	48.40	49.62	41.58	825.19	846.09	709.01
	5	3	C_1	0.25	0.17	7.27	50.59	51.98	42.74	863.39	887.19	729.47
$Ag_2O_m^+$	1	2	C_{2v}	2.82	0.45	6.30	37.60	38.09	36.98	642.89	651.42	632.39
	2	2	C_2	0.20	0.00	6.03	41.82	42.77	40.59	715.54	731.76	694.45
	3	4	C_1	0.24	2.11	6.23	51.13	52.24	45.81	875.23	894.19	784.22
	4	4	C_1	0.20	2.08	5.83	55.48	57.08	49.27	950.18	977.59	843.71
	5	4	C_1	0.12	3.71	6.05	62.17	64.79	54.74	1065.1	1110.0	937.83
$Ag_3O_m^+$	1	1	D_{3h}	2.86	0.00	5.20	44.19	45.92	45.10	757.65	787.38	773.29
	2	3	C_s	0.18	0.82	5.24	52.37	54.30	48.69	898.22	931.36	835.03
	3	3	C_1	0.25	1.19	5.13	57.34	59.97	53.56	983.72	1028.8	924.03
	4	3	C_1	−0.27	0.76	5.52	65.97	69.11	57.98	1132.0	1185.9	994.64
	5	3	C_1	−0.18	1.00	5.36	70.24	73.92	62.70	1205.5	1268.7	1076.1
$Ag_4O_m^+$	1	2	C_1	1.16	3.35	5.69	50.37	53.26	51.03	864.87	914.54	876.29
	2	2	C_s	0.07	4.19	5.30	59.29	61.63	57.33	1018.2	1058.3	984.48
	3	4	C_1	0.23	2.24	6.04	63.14	66.74	59.66	1084.5	1146.4	1024.7
	4	2	C_1	0.26	5.48	5.73	60.72	63.58	57.96	1043.0	1092.2	995.65
	5	4	C_1	0.13	4.03	2.99	76.24	81.53	69.07	1309.8	1400.6	1186.7

[a]$2S+1$: Spin multiplicity. PG: Point group symmetry. ΔE: Zero-point vibrational energy (ZPVE) corrected stabilization energy (in eV) with respect to the lowest energy dissociation channel. μ: Dipole moment at the center of mass (in Debye). VEA: Vertical electron affinity (in eV). Ω: Collision cross-section (in Å^2). Z^{-1}: Inverse electrical mobility (in V s m^{-2}). PA: Projection approximation method. EHSS: Exact hard spheres scattering method. TM: Trajectory method.

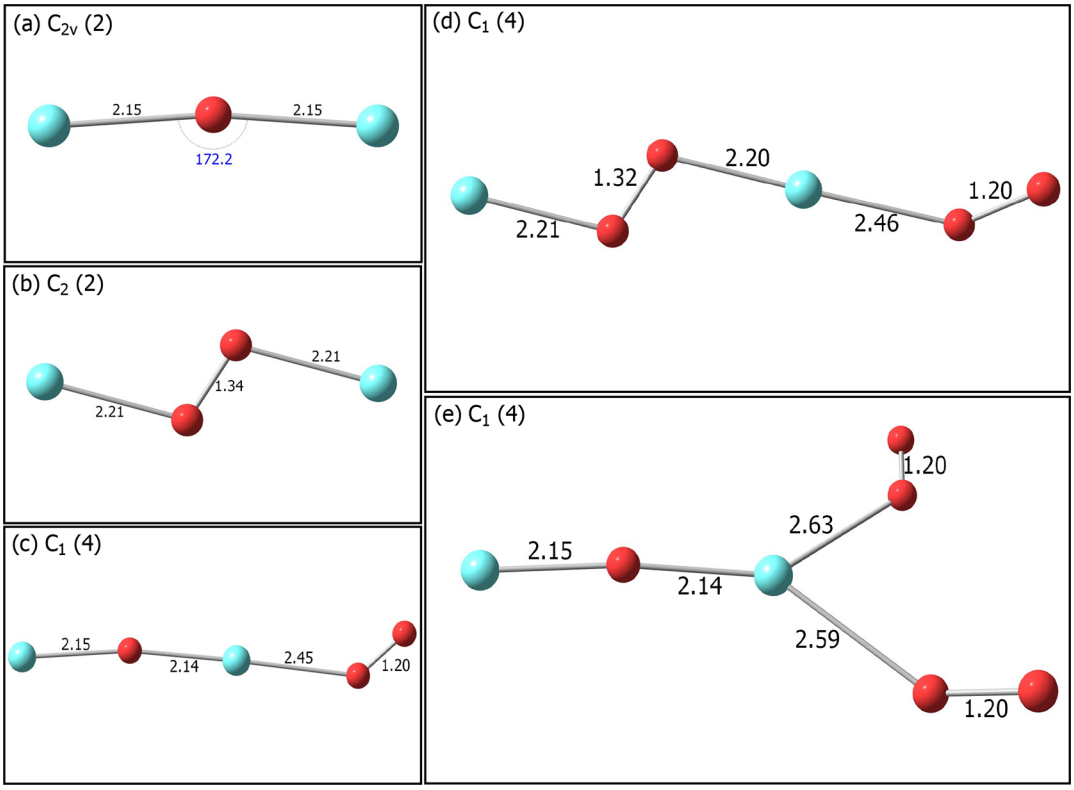

Figure 2. Ground-state structures of the $Ag_2O_m^+$ clusters optimized by the CCSD method, where m = 1−5. Red spheres denote oxygen atoms, and cyan spheres indicate silver atoms. Bond lengths (black fonts) and angles (blue fonts) are given in ångstroms and degrees, respectively. Spin multiplicities are provided in parentheses.

the ground state tends to have a greater spin multiplicity; i.e., triplet (for an even number of electrons) and quartet (for an odd number of electrons) spin states are favored over singlet and doublet states (see Table 2). More specifically, for AgO_m^+ and

https://doi.org/10.1021/acs.jpca.2c02809
J. Phys. Chem. A 2022, 126, 6376−6386

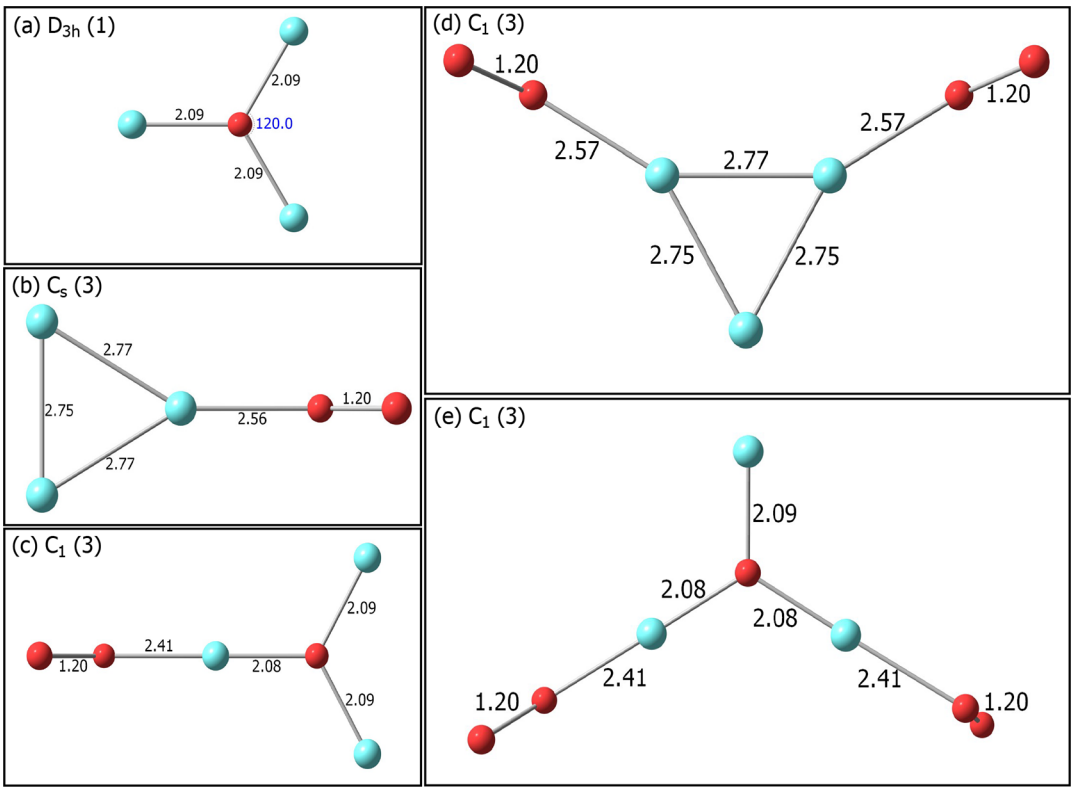

Figure 3. Ground-state structures of the $Ag_3O_m^+$ clusters optimized by the CCSD method, where $m = 1-5$. Red spheres denote oxygen atoms, and cyan spheres indicate silver atoms. Bond lengths (black fonts) and angles (blue fonts) are given in ångstroms and degrees, respectively. Spin multiplicities are provided in parentheses.

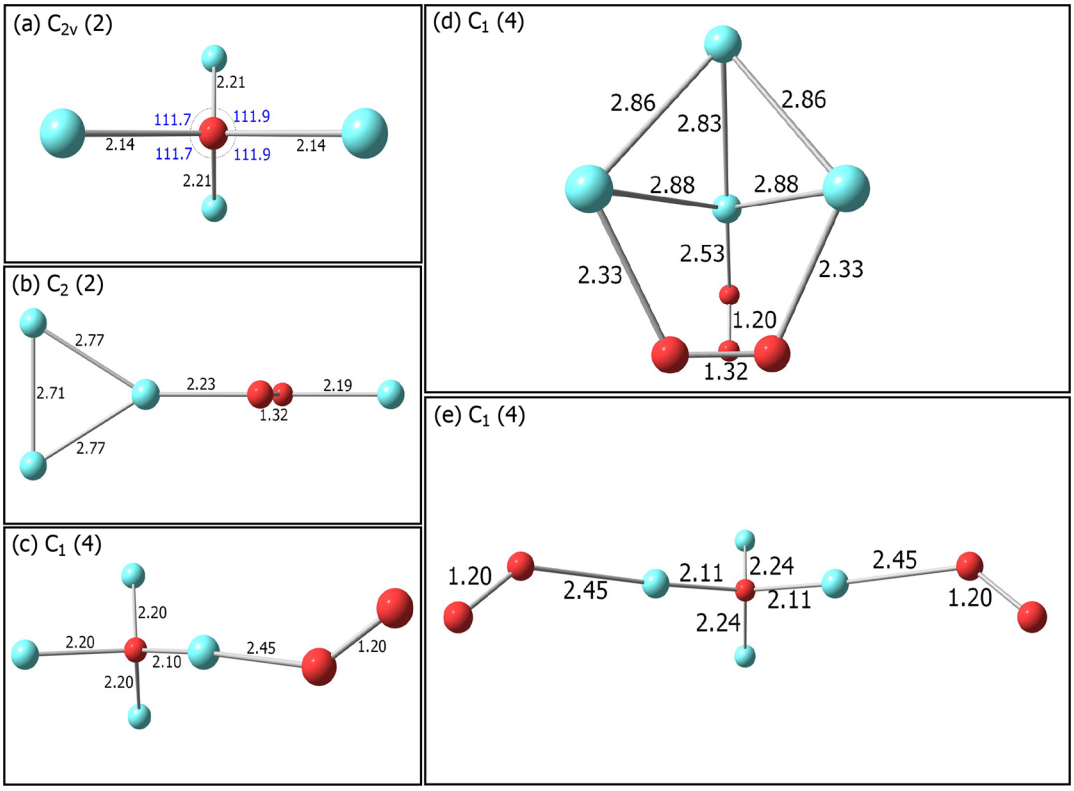

Figure 4. Ground-state structures of the $Ag_4O_m^+$ clusters optimized by the CCSD method, where $m = 1-5$. Red spheres denote oxygen atoms, and cyan spheres indicate silver atoms. Bond lengths (black fonts) and angles (blue fonts) are given in ångstroms and degrees, respectively. Spin multiplicities are provided in parentheses.

https://doi.org/10.1021/acs.jpca.2c02809
J. Phys. Chem. A 2022, 126, 6376−6386

$Ag_3O_m^+$, only one singlet state has been found in each series. On the other hand, the two smallest clusters in the series of $Ag_2O_m^+$ and $Ag_4O_m^+$ are doublets.

The geometry of the clusters in their ground state is planar if the total number of atoms in the cluster is equal to or less than four. The remaining clusters adopt a 3D structure. This is markedly different to the results reported by Roithová et al.[33] and Wang et al.,[34] where $Ag_nO_m^+$ clusters are 3D starting from tetra-atomic systems.

Interestingly, when $m \geq 2$, the $Ag_nO_m^+$ clusters have a terminal O_2 fragment attached to an Ag atom. The O−O bond length in these clusters has a length of 1.20 Å, which is almost equal to that of the free O_2 molecule (1.21 Å).[67] In these clusters, the Ag−O bond lengths are elongated (2.41−2.57 Å) compared to those of the pure AgO molecule (2.0 Å).[67] These results suggest that O_2 is weakly bonded to the $Ag_nO_{m-2}^+$ clusters and can, therefore, dissociate more easily, as discussed further below. A consequence of the weakly bounded O_2 is that the minimum energy geometry of a particular series of $Ag_nO_m^+$ is similar to that of the $Ag_nO_{m-2}^+$ clusters, with the exception of the case where an additional O_2 is attached to a terminal Ag atom. These observations are consistent for all $Ag_nO_m^+$ clusters studied in this work when the number of Ag atoms in the cluster remains the same. However, there are some notable deviations when the two oxygen atoms are bonded with two separate Ag atoms, and there is no O_2 moiety at the extremity ($Ag_2O_2^+$ and $Ag_4O_2^+$; see Figures 2b and 4b). In these two cases, the O−O distance is slightly elongated (ranging from 1.32 to 1.34 Å), and the Ag−O distance is shortened (from 2.19 to 2.23 Å) when compared to other clusters with $m \geq 2$.

Our results also show that the Ag−O bond length in the AgO^+ cluster is 2.34 Å (Figure 1a) but increases to 2.52 Å for AgO_2^+ (Figure 1b). In AgO_3^+, the Ag−O bonds are further elongated to 2.60−2.61 Å, while the distance in the O−O bond increases compared to that of AgO_2^+ (from 1.20 to 1.25 Å, respectively) (Figure 1c). We note that AgO_3^+ has a planar geometry and only a slight difference in the two Ag−O bond lengths, thus deviating from a C_{2v} point group symmetry. An incremental difference in the Ag−O bond length between Ag_2O^+ (Figure 2a) and $Ag_2O_2^+$ (Figure 2b) (2.15 and 2.21 Å, respectively) is also observed. With the exception of the linear AgO^+ ion, the most symmetric structure (in terms of the total number of symmetry operations) found in this study is that of the Ag_3O^+ cluster, which has a trigonal planar geometry with a short AgO bond length (2.09 Å; see Figure 3a). On the other hand, the $Ag_3O_2^+$ cluster can be considered as Ag atoms sitting at the corners of an equilateral triangle having sides with a length of ∼2.8 Å, with one of them being attached to an O_2 molecule (Figure 3b). Interestingly, the positively charged pure Ag_3^+ ion is also an equilateral triangle with similar side lengths, as reported by McKee and co-workers.[21] Therefore, the ground state of the $Ag_3O_2^+$ cluster can be considered as the combination of Ag_3^+ and O_2 fragments in close proximity. Similarly, the $Ag_4O_2^+$ cluster (Figure 4b) has a structure similar to that of $Ag_3O_2^+$, with the fourth Ag atom attached to the terminal O atom of the O_2 moiety.

Some discrepancies are observed by comparing the geometries determined in our study with those already reported in the literature. Most notably, we find that the ground state of the Ag_2O^+ cluster (Figure 2a) is almost linear with ∠AgOAg = 172.2°, which is in line with the results reported by Roithová et al.[33] but in contrast with those provided by Schmidt et al.[18] and Wang et al.[34] The energy of this structure is at least 0.18 eV (0.13 eV for M06 calculations in this work) lower compared to that of the bent structure as obtained in the two latter studies. Indeed, we find that both PBE and LSDA functionals (with the same basis set as employed in this study) refer to the ground state having a bent geometry, which has respectively at least 0.07 and 0.28 eV lower energy compared to that of the linear geometry. We find that the Ag−O bond length is also marginally longer (2.15 Å) than those previously reported by Schmidt et al. and Wang et al. (2.09 and 1.98 Å, respectively).

Similarly, Schmidt et al. and Wang et al. reported that the ground state of Ag_3O^+ (Figure 3a) and Ag_4O^+ (Figure 4a) clusters have respectively a tetrahedron-like and capped tetrahedron geometry, both belonging to the C_{3v} point group symmetry. In contrast, we find that the ground state of these clusters belongs to the D_{3h} (Ag_3O^+) and C_1 (Ag_4O^+) symmetric configurations, which have 0.40 and 0.15 eV, respectively, lower energy than the previously reported C_{3v} geometries. We should note, however, that the Ag_4O^+ cluster marginally deviates by an Ag−O bond length of ±0.07 Å (see Figure 4a) from having a pure tetrahedral geometry. Additional geometrical discrepancies are also seen for the $Ag_2O_2^+$ (Figure 2b) and $Ag_4O_2^+$ (Figure 4b) clusters. These discrepancies may stem from the difference in the accuracy of the *ab initio* methods employed, the convergence criteria, or the total number of candidate structures and their geometries considered in the respective studies. Nevertheless, we have found good agreement with the previous reports for a few species, including the AgO_2^+ (Figure 1b) and $Ag_3O_2^+$ (Figure 3b) clusters.

In addition to the ground-state geometries, we have also determined other properties of the oxidized silver clusters, such as the dipole moment μ and the vertical electron affinity (VEA). The calculated values are provided in Table 2. Since the dipole moment of an electrically charged species is not invariant under the choices of the coordinate frame, it has been calculated at the center of mass of the cluster. The direction of the dipole vectors is fully consistent with the partial charges determined by the NPA method; i.e. they point toward the plane containing the positively charged Ag atom(s) (see SI for charges calculated by the NPA method on the $Ag_nO_m^+$ clusters). As expected, some symmetric structures, such as those of $Ag_2O_2^+$ (Figure 2b) and Ag_3O^+ (Figure 3a), have zero net dipole moments. The $Ag_4O_m^+$ clusters appear to have higher dipole moments than other $Ag_nO_m^+$ series, most likely due to a greater number of partially charged Ag atoms located away from the center of mass (Figure 4a). Finally, the VEA values can be distinctly categorized with respect to the value of n. For $n = 1-3$, the VEA values decrease as n increases. For example, the VEAs span from 6.9 to 7.4 eV for the AgO_m^+ series but decrease to the range of 5.8−6.2 eV for the $Ag_2O_m^+$ clusters and to 5.1−5.5 eV for the $Ag_3O_m^+$. Interestingly, the VEAs of the $Ag_4O_m^+$ clusters are spread over a rather broad range: i.e., from 6.0 eV for $Ag_4O_3^+$ to 3.0 eV for $Ag_4O_5^+$.

3.2. Stabilization Energies of the $Ag_nO_m^+$ Clusters. The ZPVE corrected ΔE of the $Ag_nO_m^+$ clusters are provided in Table 2 and shown in Figure 5a. Evidently, the stabilization of the clusters with $m \geq 2$ is comparatively lower than those with $m = 1$. These clusters preferably dissociate by eliminating a weakly bonded oxygen molecule. The calculated ΔE values for the clusters with $m \geq 2$ range from approx. − 0.27 to 0.28 eV, suggesting that some clusters are unstable ($\Delta E \leq 0$; viz., AgO_4^+, $Ag_3O_4^+$, and $Ag_3O_5^+$) and will promptly dissociate. The ΔE values of most of the remaining $Ag_nO_m^+$ clusters (with $m \geq 2$) have a value of ∼0.2 eV. One exception to this generalization is the AgO_3^+ cluster, for which the calculated stabilization energy is significantly greater than those of other clusters (∼0.8 eV). We

https://doi.org/10.1021/acs.jpca.2c02809
J. Phys. Chem. A 2022, 126, 6376−6386

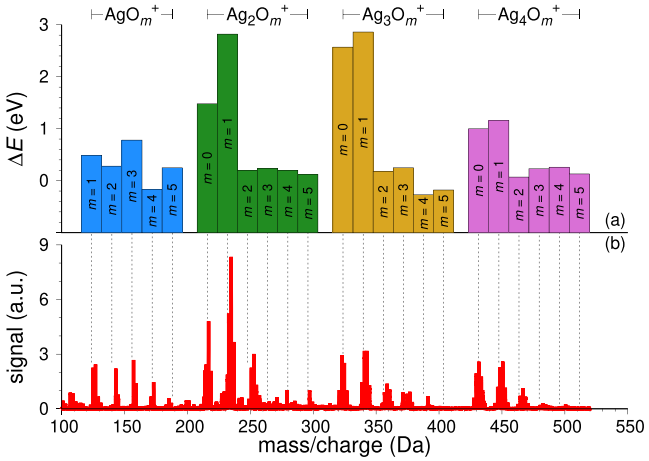

Figure 5. (a) Stabilization energies, ΔE, of the $Ag_nO_m^+$ clusters (n = 1−4 and m = 0−5) with respect to the lowest energy dissociation channel. The ΔE values are calculated by the CCSD(T) method. (b) Mass spectra of atomic silver clusters produced by atmospheric-pressure spark ablation provided by Maisser et al. (ref 43). The abscissa of panel (a) has the same value, unit, and label as that of panel (b).

should highlight here that in AgO_3^+, the Ag atom is directly bonded with two O atoms, and the third O atom is centrally bonded with those (see Figure 1c). We determine that this ion will most readily dissociate not through the release of O_2 but of an ozone molecule and a silver cation Ag^+. Dissociation of AgO_3^+ to yield $AgO^+ + O_2$ would require surmounting a potential energy barrier of around 1.1 eV. The ΔE values for $Ag_nO_2^+$ clusters calculated in this work are considerably smaller (i.e., less stable clusters) than the O_2 binding energy reported by Wang et al.[34] For example, we estimate that the binding energy of O_2 on $Ag_2O_2^+$ is 0.2 eV, whereas Wang and co-workers report a value of 1 eV.

With the exception of AgO_3^+, the stabilization energy of the Ag_nO^+ clusters is, in general, far larger than those of the clusters with $m \geq 2$ (see Table 2). This finding is consistent with those reported by Schmidt et al.[68] in the condensed phase, who showed that the detection intensity of Ag_nO^+ clusters was substantially higher than that of their $Ag_nO_2^+$ counterparts. ΔE of Ag_2O^+ and Ag_3O^+ have similar values (~2.8 eV) and are notably larger than those of AgO^+ (0.5 eV) and Ag_4O^+ (1.2 eV), in agreement with previous DFT level calculations reported by Schmidt and co-workers[18] and Roithová et al.[33] The enhanced stabilization energy of the Ag_2O^+ and Ag_3O^+ clusters can seemingly be attributed to a stronger Coulombic interaction between partially positive Ag atoms surrounding the negatively charged O atoms at a shorter distance (cf., Figure S1 for charges calculated by the NPA method for the Ag_nO^+ clusters). Interestingly, in the equilibrium geometry of AgO^+, there is no net charge on the O atom. This suggests that there is no effective Ag to O charge transfer in AgO^+, in contrast to the neutral AgO cluster, whereas the potential energy curve of AgO^+ has a shallow well of ~0.5 eV (see Figure S2). The bond dissociation energy of Ag^+−O reported here is somewhat smaller than the purely speculative experimental value of 1.23 ± 0.05 eV,[24] or the DFT calculated values reported by Wang and co-workers,[34] but have a better agreement with those provided by Schmidt (≈0.8 eV). For n = 2 and 4, the lowest energy dissociation channel leads to the formation of a silver cluster cation and a single O atom ($Ag_nO^+ \rightarrow Ag_n^+ + O$). In contrast, Ag_3O^+ would preferably dissociate into $Ag_2O^+ + Ag$, which has a 0.2 eV lower energy than the $Ag_3^+ + O$ channel.

Figure 5a shows the stabilization energies of the $Ag_nO_m^+$ clusters predicted in this work, whereas Figure 5b provides the mass spectra (MS) of Ag-based cations reported by Maisser et al.[43] As the signal strength in the experimentally determined MS can be a measure of relative abundances and consequently related to the relative stabilization energy of the clusters, we can qualitatively compare them with the theoretically determined stabilization energies. In all cases, the mass spectrometry signals of $Ag_nO_m^+$ clusters for $n > 1$ and $m \geq 2$ are weaker than those obtained for m = 0 or 1. These signals progressively become weaker with increasing m. This is, in general, in agreement with the calculated stabilization energies of the $Ag_nO_m^+$ clusters and the experimental validation by Schmidt et al.[18] Similarly, AgO_m^+ clusters with m = 1, 2, and 3 have comparable signal strengths in the MS, in accordance with the corresponding ΔE values. By comparing the stabilization energies of the pure Ag_n^+ clusters (i.e., Ag_2^+, Ag_3^+, and Ag_4^+) with respect to the lowest energy dissociation channel ($Ag_{n-1}^+ + Ag$ for even n, and $Ag_{n-1} + Ag^+$ for odd n) with those obtained for Ag_nO^+ (n = 2−4), we can interpret the remaining peaks of the MS. For instance, the ΔE of Ag_2O^+ is much greater than that of the Ag_2^+ ion (2.82 and 1.48 eV, respectively), which can explain the stronger signal in the case of the oxidized species. On the other hand, the difference in ΔE between Ag_3O^+ and Ag_3^+ (2.86 and 2.57 eV, respectively) or Ag_4O^+ and Ag_4^+ (1.16 and 1.00 eV, respectively) pairs are very small and consequently can explain the similar magnitudes of the respective signals in the MS. These comparisons show that as the silver clusters increase in size, they have a smaller tendency to react with oxygen. Formation of predominantly pure silver is to be expected for clusters with $n \geq 10$. It should be noted that the ΔE values of the pure Ag_n^+ clusters have also been determined at the CCSD(T) theory with ZPVE correction. Despite the excellent qualitative agreement between measurements and calculations, one should also consider that the MS have contributions from hydroxy silver cluster cations, $Ag_nOH_m^+$, as shown by Maisser et al.[43] To properly interpret the experimental MS, one would need to estimate the stabilities of the $Ag_nOH_m^+$ clusters and additionally conduct kinetic studies on pure, oxygenated, and hydroxygenated silver cluster cations in order to determine their relative abundances. This, however, is beyond the scope of this study.

3.3. Collision Cross Sections and Electrical Mobilities of the $Ag_nO_m^+$ Clusters. The average CCSs for the $Ag_nO_m^+$ clusters calculated by the PA, EHSS, and TM methods are provided in Table 2. In the remainder of this article, we specifically analyze results obtained by the TM approach as this has been reported to provide the most accurate results among the three methods and, most importantly, because it considers the long-range interactions between the ion and the buffer gas.[40] As the CCS is essentially a measure of cluster size, it increases as the number of oxygen atoms in a family of $Ag_nO_m^+$ increases. One deviation from this generalization is observed for the $Ag_4O_4^+$ cluster, which has a smaller CCS value than its $Ag_4O_3^+$ counterpart that has one oxygen atom less (57.96 and 59.66 Å^2, respectively). This anomaly can be explained by carefully inspecting the corresponding optimized geometries of the $Ag_4O_3^+$ and $Ag_4O_4^+$ ions. As already shown in Figure 4d, the ground state of $Ag_4O_4^+$ is a compact cage-like structure with a total molecular area of 47.30 Å^2, whereas $Ag_4O_3^+$ (Figure 4c) has a more spread-out geometry and an increased molecular area (50.76 Å^2).

https://doi.org/10.1021/acs.jpca.2c02809
J. Phys. Chem. A 2022, 126, 6376−6386

Figure 6 shows the experimentally determined inverse mobility Z^{-1} spectrum measured by Maisser et al.,[13] where

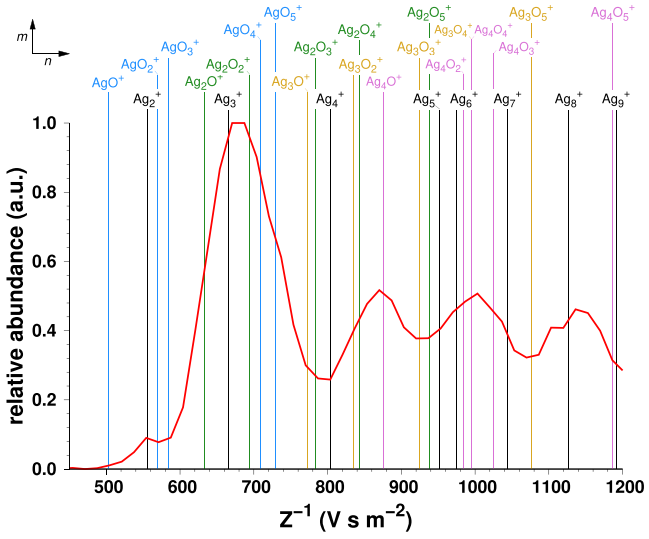

Figure 6. Inverse electrical mobility, Z^{-1}, (in V s m^{-2}) of $Ag_nO_m^+$ clusters (n = 1−4; m = 1−5) and Ag_n^+ clusters (n = 2−9) in He calculated at 20 °C and 1 atm. Z^{-1} values of $Ag_nO_m^+$ clusters have been calculated by the trajectory method (TM), and for Ag_n^+, the clusters are based on the experimental collision cross sections reported in the literature (ref 17). They are both labeled as vertical lines on the experimental mobility spectrum provided by Maisser et al. (solid red lines, ref 13).

respective values of the oxidized and pure (the latter taken from ref 17) silver cluster cations are also labeled. The calculated values of Z^{-1} are also provided in Table 2. We should note that the Z^{-1} values for Ag_n^+ clusters are marginally smaller than those provided by Maisser et al.[13] because they account for particularities in the calibration procedure used in the experiments. Similarly to the CCS, Z^{-1} increases with m for a particular series of $Ag_nO_m^+$ clusters, except for $Ag_4O_4^+$ due to its smaller size compared to $Ag_4O_3^+$ as discussed in the previous paragraph.

A number of peaks and troughs that were previously unassigned in the experimental electrical mobility spectrum can now be labeled as belonging to a family of cationic clusters. For example, in the case of AgO_2^+, the inverse mobility that coincides with the first experimental peak at Z^{-1} = 570 V s m^{-2} appears alongside the signal corresponding to the Ag_2^+ cluster. Similarly, the most prominent peak at $Z^{-1} \approx 700$ V s m^{-2} has contributions from both Ag_3^+ and $Ag_2O_2^+$. The following two peaks at larger Z^{-1} values of around 870 and 1000 V s m^{-2} that are also labeled, respectively, contain the family of $Ag_4O_m^+$ (m = 1−4) and the AgO_4+ clusters. Likewise, the troughs appearing around 800, 950, and 1100 V s m^{-2} correspond to Ag_3O^+ and $Ag_2O_3^+$, $Ag_3O_3^+$, and $Ag_2O_5^+$, and $Ag_3O_5^+$ clusters, respectively.

It is evident that the relative abundances of the $Ag_nO_m^+$ clusters labeled on the experimental electrical mobility spectrum do not precisely match the calculated stabilization energies, contradicting the comparison with the reported MS discussed in the previous section. This is particularly true for the Ag_3O^+ cluster. The stabilization energy of Ag_3O^+ is 2.86 eV exhibiting the highest ΔE value compared to the rest of the species investigated in this work, corroborating the strong signal in the MS reported by Maisser et al.[43] However, Ag_3O^+ falls at a trough in the experimentally determined electrical mobility spectrum, which may suggest that the ground state of Ag_3O^+ would dissociate rapidly. This seemingly contradictory observation could be the result of one or a combination of the following factors. First, there could be isomers of Ag_3O^+ that are sufficiently long-lived and have ion mobilities that fall under the adjacent peaks in the mobility spectrum. We have calculated that the tetrahedron-like structure reported by Schmidt et al.[18] and Wang et al.,[34] and the first triplet state of Ag_3O^+ (cf., Figure S3) have a Z^{-1} value of 744 V s m^{-2}. This value, which is lower than that estimated for the D_{3h} structure (corresponding to 773 V s m^{-2}) may signify a greater abundance of these two isomers. Second, it has been reported that for small and medium ions, when optimized Lennard-Jones parameters are used in the computation of CCS, the accuracy of the TM method of the MOBCAL code usually falls within 4% of the experimental value.[61,69] Due to the lack of experimental data on either CCS or electrical mobility of silver oxide cations, we have utilized nonoptimized Lennard-Jones parameters in this study. Lastly, the signals in both the mass and the electrical mobility spectra are affected by the penetration of the instruments, which can well depend on the mass and mobility of the measured clusters, respectively.

To further investigate the agreement between the theoretical calculations carried out here and the respective mobility measurements reported by Maisser et al.,[13] we compare the predicted mobility distributions determined from the signal strength of the MS of ref 43 (cf., Figure S4). Evidently, there is a good agreement between the measured and the predicted inverse mobility spectrum. However, few notable differences are also observed since the electrical mobility and the mass spectra measurements have been performed separately, and hence, important differences in the composition of the resulting clusters cannot be ruled out. The most prominent discrepancy arises for the Ag_2^+ cluster as its relative abundance is 0.9 au in the predicted mobility spectrum and 0.1. a.u. in the experimental spectrum. Remarkably, Ag_3O^+ falls at a peak in the predicted mobility spectrum since it is accompanied by a strong signal in the corresponding MS. Unsurprisingly, Ag_3^+, Ag_3O^+, Ag_4^+, and Ag_4O^+ clusters have similar relative abundances and signal strengths in the predicted mobility and the experimental spectra.

The weakening signal with growing cluster size (Figure 6) can also be connected to experimental artifacts. First, the transmission of the clusters through the mass spectrometer is mass-dependent and, in principle, decreases with increasing mass. In addition, clusters produced by spark ablation typically have a log-normal mobility/size distribution,[43] which also leads to a size-dependent signal of the clusters that can vary with the operating parameters of their production during the experiments. Finally, we should stress again that the Ag-based clusters produced during the experiments contain a high fraction of hydroxyls, resulting to species that can be more stable than their $Ag_nO_m^+$ cluster counterparts. To make a quantitative comparison between theory and experiment, we need to consider those clusters as well as their mass/size-dependent penetrations in the MS measurements.

The deviation in the ion mobilities between the pure Ag_n^+ cluster and its oxidized counterparts having the same number of silver atoms n can give valuable insights into the amount of oxidation, i.e., the total number of O atoms, in the cluster. Figure 7 shows the difference in inverse mobility Z^{-1} between pure Ag_n^+ clusters with their oxygenated counterparts, $Ag_nO_m^+$ for a particular value of n against m. Naturally, with increasing the

https://doi.org/10.1021/acs.jpca.2c02809
J. Phys. Chem. A 2022, 126, 6376−6386

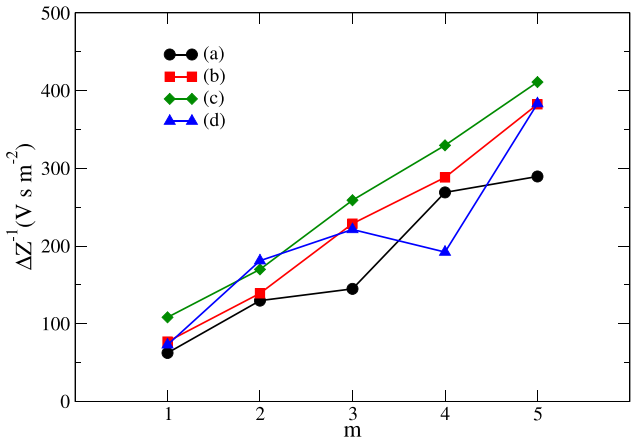

Figure 7. Difference in inverse electrical mobility, ΔZ^{-1}, (in V s m^{-2}) between (a) Ag^+ and AgO_m^+, (b) Ag_2^+ and $Ag_2O_m^+$, (c) Ag_3^+ and $Ag_3O_m^+$, and (d) Ag_4^+ and $Ag_4O_m^+$. Here, m = 1−5. Z^{-1} values of $Ag_nO_m^+$ clusters have been calculated by the trajectory method (TM), and for Ag_n^+, the clusters are based on the experimental collision cross sections reported in the literature (ref 17).

number of oxygen atoms in the cluster, ΔZ^{-1} increases as a result of the larger cluster size, except for the $Ag_4O_4^+$ cluster.

The large difference in the ΔZ^{-1} values between Ag_n^+ and $Ag_nO_m^+$ clusters can be explained by inspecting their respective ground-state geometries. For example, Ag_2O^+, Ag_3O^+, and Ag_4O^+ can be considered as structures in which an oxygen atom is placed at the center of pure Ag_2^+, Ag_3^+, and Ag_4^+ clusters, respectively (see Figure S5). This leads to an increased Ag − Ag bond length in the oxidized clusters compared to their pure counterparts (by 0.74−1.45 Å) and, in general, a larger cluster size. Since the significant contribution to the electrical mobility originates from the larger Ag atoms, it is not surprising that adding an O atom has a much smaller effect on the electrical mobility than adding an Ag atom. The deviation of the mobility of the $Ag_nO_m^+$ species from their pure counterparts is high enough to be resolved by mobility analysis reported by Maisser et al.,[13] as this ranges from 24 to 160 V^{-1} s^{-1} cm^2 depending on the number of O atoms the clusters can contain for our study. Since the mobilities of some oxygenated species are very close to those of the pure clusters, and also among themselves, two or more species can correspond to each peak in the mobility spectrum obtained from low resolution DMA, as shown in Figure 6. For example, $Ag_3O_4^+$ has a Z^{-1} value of 994.64 V s m^{-2}, which is very close to the respective value calculated for $Ag_4O_4^+$ (995.65 V s m^{-2}). Similarly, $Ag_4O_5^+$ and Ag_9^+ have comparable Z^{-1} values (∼1190 V s m^{-2}). In order to better resolve different oxidized species and have a more rigorous comparison with the theoretical results, one can combine mobility classification with mass spectrometry that can give further insights into the relationship between cluster mobility, mass, sizes, and stability.[70,71]

4. CONCLUSIONS

We have calculated the minimum energy structures, stabilization energy, electrical mobilities and various electronic properties of $Ag_nO_m^+$ clusters (n = 1−4; m = 1−5) using a rigorous *ab initio* method. Geometry optimizations of the $Ag_nO_m^+$ clusters have been performed at the CCSD level of theory, while single-point energies are determined by additionally incorporating the triples correction to the CCSD method (CCSD(T)). We find that the ground state of the larger cations tends to have a greater multiplicity. In general, the ground state geometry of the $Ag_nO_m^+$ clusters is similar to those of the $Ag_nO_{m-2}^+$ clusters, with an additional O_2 attached at their extremity, although there are some exceptions to this rule (e.g., $Ag_2O_2^+$ and $Ag_4O_2^+$). The Ag_nO^+ clusters adopt a geometry that inherits higher symmetry than other clusters and also has greater stabilization energy with respect to the lowest energy dissociation channel. This is apparently due to a strong Coulombic attraction between positively charged Ag atoms and a negatively charged O atom. On the other hand, $Ag_nO_m^+$ clusters with $m \geq 2$ are less stable due to the easy elimination of an O_2 molecule attached to a terminal Ag atom, signaling a higher inertness of the silver clusters toward oxygen. We expect that this is a general feature and that larger clusters also split off O_2. Under this hypothesis and considering that even the bulk stable Ag_2O decomposes when heated,[72] it is well possible that silver oxide clusters produced by spark ablation (or other similar aerosol-based techniques) at atmospheric pressure can be reduced by heating their carrier gas, leading to an effective yet cost-effective way of producing pure silver clusters.

When comparing the structures of the oxidized silver clusters determined in this work with those previously obtained by DFT calculations, we find a number of disparities, e.g., in the case of the Ag_2O^+ cluster. Through more rigorous computations, we find that the ground-state structure of Ag_2O^+ is almost linear, in contrast to the bent geometry reported previously. Despite these discrepancies, however, the good qualitative agreement with experimentally determined mass spectra[43] builds trust in the *ab initio* calculations caried-out in this work.

The collision cross-section (CCS) and electrical mobilities of the $Ag_nO_m^+$ clusters have also been calculated and labeled on a measured spectrum of silver-based atomic clusters produced by spark ablation at atmospheric pressure.[13] This comparison provides further insights into the species that can contribute to each peak of the measured mobility spectrum and verify the calculations that depend on the estimated structure of different clusters. Finally, estimated deviations in the ion mobilities of the pure silver cluster cations from their oxidized counterparts indicate that the resolving power of the measured mobility spectrum is high enough to distinguish between clusters having a different number of Ag atoms but not between clusters having the same number of Ag atoms and a different number of oxygen atoms since they appear in the same region of the mobility spectrum and consequently a peak or a trough may be the result of the presence or absence of more than one species. This limitation can be overcome by using accurate quantum chemical calculations or Differential Mobility Analysis-Mass Spectrometry (DMA-MS) in the future.

■ ASSOCIATED CONTENT

Supporting Information

The Supporting Information is available free of charge at https://pubs.acs.org/doi/10.1021/acs.jpca.2c02809.

Coordinates of optimized geometries of $Ag_nO_m^+$ clusters, atomic charges of Ag_nO^+ determined by NPA, CCSD(T) potential energy curves of AgO and AgO^+, first triplet state geometry of the Ag_3O^+ cluster, and geometry and bond distances of Ag_n^+ and Ag_nO^+ clusters (PDF)

https://doi.org/10.1021/acs.jpca.2c02809
J. Phys. Chem. A 2022, 126, 6376−6386

AUTHOR INFORMATION

Corresponding Author

George Biskos − *Climate & Atmosphere Research Centre, The Cyprus Institute, Nicosia 2121, Cyprus; Faculty of Civil Engineering and Geosciences, Delft University of Technology, Delft 2628 CN, The Netherlands*; Phone: +357 22 208618; Email: g.biskos@cyi.ac.cy; Fax: +357 22208625

Authors

Somnath Bhowmick − *Climate & Atmosphere Research Centre, The Cyprus Institute, Nicosia 2121, Cyprus;* orcid.org/0000-0001-7498-2463

Anne Maisser − *Climate & Atmosphere Research Centre, The Cyprus Institute, Nicosia 2121, Cyprus*

Yury V. Suleimanov − *Computation-Based Science and Technology Research Center, The Cyprus Institute, Nicosia 2121, Cyprus;* orcid.org/0000-0001-9978-2791

Andreas Schmidt-Ott − *Climate & Atmosphere Research Centre, The Cyprus Institute, Nicosia 2121, Cyprus; Faculty of Applied Sciences, Delft University of Technology, Delft 2629 HZ, The Netherlands*

Complete contact information is available at: https://pubs.acs.org/10.1021/acs.jpca.2c02809

Notes

The authors declare no competing financial interest.

ACKNOWLEDGMENTS

The authors acknowledge the financial support of the European Regional Development Fund and the Republic of Cyprus through the Research Promotion Foundation NANO^{2}LAB Project INFRASTRUCTURES/1216/0070. This research was also supported by the EMME-CARE project that has received funding from the European Union's Horizon 2020 Research and Innovation Program, under Grant Agreement No. 856612, as well as matching cofunding by the Government of the Republic of Cyprus. The authors thank the AMD EPYC High Performance Computing Facility of The Cyprus Institute for computational resources.

REFERENCES

(1) Alexander, J. W. History of the Medical Use of Silver. *Surg. Infect.* **2009**, *10*, 289−292.

(2) Grier, N. In *Disinfection, Sterilization and Preservation*; Block, S. S., Ed.; Lea & Febige, 1968; pp 375−398.

(3) Lemire, J. A.; Harrison, J. J.; Turner, R. J. Antimicrobial Activity of Metals: Mechanisms, Molecular Targets and Applications. *Nat. Rev. Microbiol.* **2013**, *11*, 371−384.

(4) Koretsky, G. M.; Knickelbein, M. B. The Reactions of Silver Clusters with Ethylene and Ethylene Oxide: Infrared and Photoionization Studies of $Ag_n(C_2H_4)_m$, $Ag_n(C_2H_4O)_m$ and their Deuterated Analogs. *J. Chem. Phys.* **1997**, *107*, 10555−10566.

(5) Curtiss, L.; Greeley, J.; Vajda, S. Tiny Trimer, Big Result. *The Chemical Engineer* **2010**, No. 829/830, 46−48.

(6) Lee, K.-S.; El-Sayed, M. A. Gold and Silver Nanoparticles in Sensing and Imaging: Sensitivity of Plasmon Response to Size, Shape, and Metal Composition. *J. Phys. Chem. B* **2006**, *110*, 19220−19225.

(7) Caro, C.; Castillo, P. M.; Klippstein, R.; Pozo, D.; Zaderenko, A. P. In *Silver Nanoparticles*; Perez, D. P., Ed.; IntechOpen, 2010; Chapter 11. DOI: 10.5772/8513.

(8) Kim, S.-H.; Medeiros-Ribeiro, G.; Ohlberg, D. A. A.; Williams, R. S.; Heath, J. R. Individual and Collective Electronic Properties of Ag Nanocrystals. *J. Phys. Chem. B* **1999**, *103*, 10341−10347.

(9) Borsella, E.; Cattaruzza, E.; De Marchi, G.; Gonella, F.; Mattei, G.; Mazzoldi, P.; Quaranta, A.; Battaglin, G.; Polloni, R. Synthesis of Silver Clusters in Silica-based Glasses for Optoelectronics Applications. *J. Non-Cryst. Solids* **1999**, *245*, 122−128.

(10) Novikov, S. M.; Popok, V. N.; Evlyukhin, A. B.; Hanif, M.; Morgen, P.; Fiutowski, J.; Beermann, J.; Rubahn, H.-G.; Bozhevolnyi, S. I. Highly Stable Monocrystalline Silver Clusters for Plasmonic Applications. *Langmuir* **2017**, *33*, 6062−6070.

(11) Pereiro, M.; Baldomir, D.; Botana, J.; Arias, J. E.; Warda, K.; Wojtczak, L. Biomedical Applications of Small Silver Clusters. *J. Appl. Phys.* **2008**, *103*, 07A315.

(12) Hsu, H.-C.; Lin, Y.-X.; Chang, C.-W. The Optical Properties of the Silver Clusters and their Applications in the Conformational Studies of Human Telomeric DNA. *Dyes Pigm* **2017**, *146*, 420−424.

(13) Maisser, A.; Barmpounis, K.; Attoui, M. B.; Biskos, G.; Schmidt-Ott, A. Atomic Cluster Generation with an Atmospheric Pressure Spark Discharge Generator. *Aerosol Sci. Technol.* **2015**, *49*, 886−894.

(14) Vons, V.; Anastasopol, A.; Legerstee, W.; Mulder, F.; Eijt, S.; Schmidt-Ott, A. Low-Temperature Hydrogen Desorption and the Structural Properties of Spark Discharge Generated Mg Nanoparticles. *Acta Mater.* **2011**, *59*, 3070−3080.

(15) Selinger, A.; Schnabel, P.; Wiese, W.; Irion, M. P. Size Distribution Studies of Sputtered Transition Metal Cluster Ions by Fourier Transform Ion Cyclotron Resonance Mass Spectrometry. *Ber. Bunsenges. Phys. Chem.* **1990**, *94* (11), 1278−1282.

(16) Fournier, R. Theoretical Study of the Structure of Silver Clusters. *J. Chem. Phys.* **2001**, *115*, 2165−2177.

(17) Weis, P.; Bierweiler, T.; Gilb, S.; Kappes, M. M. Structures of Small Silver Cluster Cations (Ag_n^+, $n < 12$): Ion Mobility Measurements Versus Density Functional and MP2 Calculations. *Chem. Phys. Lett.* **2002**, *355*, 355−364.

(18) Schmidt, M.; Cahuzac, P.; Bréchignac, C.; Cheng, H. P. The Stability of Free and Oxidized Silver Clusters. *J. Chem. Phys.* **2003**, *118*, 10956−10962.

(19) Duanmu, K.; Truhlar, D. G. Validation of Methods for Computational Catalyst Design: Geometries, Structures, and Energies of Neutral and Charged Silver Clusters. *J. Phys. Chem. C* **2015**, *119*, 9617−9626.

(20) Van Der Tol, J.; Jia, D.; Li, Y.; Chernyy, V.; Bakker, J. M.; Nguyen, M. T.; Lievens, P.; Janssens, E. Structural Assignment of Small Cationic Silver Clusters by Far-Infrared Spectroscopy and DFT Calculations. *Phys. Chem. Chem. Phys.* **2017**, *19*, 19360−19368.

(21) McKee, M. L.; Samokhvalov, A. Density Functional Study of Neutral and Charged Silver Clusters Ag_n with $n = 2 - 22$. Evolution of Properties and Structure. *J. Phys. Chem. A* **2017**, *121*, 5018−5028.

(22) Lian, L.; Hackett, P. A.; Rayner, D. M. Relativistic Effects in Reactions of the Coinage Metal Dimers in the Gas Phase. *J. Chem. Phys.* **1993**, *99*, 2583−2590.

(23) Flurer, R. A.; Busch, K. L. Structures of Ag_2X^+ and Cu_2X^+ Ions: Comparison of Theoretical Predictions with Experimental Results from Mass Spectrometry/Mass Spectrometry. *J. Am. Chem. Soc.* **1991**, *113*, 3656−3663.

(24) Chen, Y.; Armentrout, P. B. Kinetic Energy Dependence of the Reactions of Ru^+, Rh^+, Pd^+, and Ag^+ with O_2. *J. Chem. Phys.* **1995**, *103*, 618−625.

(25) Bréchignac, C.; Cahuzac, P.; Leygnier, J.; Tignères, I. Reactive Nucleation of Silver Clusters with Oxygen and Water. *Chem. Phys. Lett.* **1999**, *303*, 304−310.

(26) Socaciu, L. D.; Hagen, J.; Heiz, U.; Bernhardt, T. M.; Leisner, T.; Wöste, L. Reaction Mechanism for the Oxidation of Free Silver Dimers. *Chem. Phys. Lett.* **2001**, *340*, 282−288.

(27) Manard, M. J.; Kemper, P. R.; Bowers, M. T. Bonding Interactions in $Ag^+(O_2)_n$ and $Ag_2^+(O_2)_n$ Clusters: Experiment and Theory. *Int. J. Mass Spectrom.* **2003**, *228*, 865−877.

(28) Snyders, R.; Wautelet, M.; Gouttebaron, R.; Dauchot, J.; Hecq, M. Experimental and Theoretical Studies of the DC Reactive Magnetron Sputtering Deposition of Silver Oxide Thin Films. *Surf. Coat. Technol.* **2003**, *174*−*175*, 1282−1286.

(29) Schmidt, M.; Masson, A.; Bréchignac, C. Oxygen and Silver Clusters: Transition from Chemisorption to Oxidation. *Phys. Rev. Lett.* **2003**, *91*, 1−4.
(30) Schmidt, M.; Masson, A.; Bréchignac, C. Enhancement of Nitrogen Physisorption in Coadsorption with Oxygen On Free, Positively Charged Silver Clusters. *J. Chem. Phys.* **2005**, *122*, 134712.
(31) Bernhardt, T. M. Gas-phase Kinetics and Catalytic Reactions of Small Silver and Gold Clusters. *Int. J. Mass Spectrom.* **2005**, *243*, 1−29.
(32) Bonacic-Koutecky, V.; Boiron, M.; Pittner, J.; Fantucci, P.; Koutecký, J. Structural and Optical Properties of Small Oxygen-Doped- and Pure-Silver Clusters. *Eur. Phys. J. D* **1999**, *9*, 183−187.
(33) Roithová, J.; Schröder, D. Gas-phase Models for Catalysis: Alkane Activation and Olefin Epoxidation by the Triatomic Cation Ag_2O^+. *J. Am. Chem. Soc.* **2007**, *129*, 15311−15318.
(34) Wang, Y.; Gong, X. G. First-Principles Study of Small Oxidized Silver Clusters. *J. Nanosci. Nanotechnol.* **2010**, *10*, 5500−5506.
(35) Perdew, J. P.; Burke, K.; Ernzerhof, M. Generalized Gradient Approximation Made Simple. *Phys. Rev. Lett.* **1996**, *77*, 3865−3868.
(36) Perdew, J. P.; Zunger, A. Self-Interaction Correction to Density-Functional Approximations for Many-Electron Systems. *Phys. Rev. B* **1981**, *23*, 5048−5079.
(37) Blöchl, P. E. Projector Augmented-Wave Method. *Phys. Rev. B* **1994**, *50*, 17953−17979.
(38) Mason, E. A.; McDaniel, E. W. *Transport Properties of Ions in Gases*; John Wiley & Sons, Inc.: New York, 1988. DOI: 10.1002/3527602852.
(39) Hagen, D. F. Characterization of Isomeric Compounds by Gas and Plasma Chromatography. *Anal. Chem.* **1979**, *51*, 870−874.
(40) Mesleh, M. F.; Hunter, J. M.; Shvartsburg, A. A.; Schatz, G. C.; Jarrold, M. F. Structural Information from Ion Mobility Measurements: Effects of the Long-Range Potential. *J. Phys. Chem.* **1996**, *100*, 16082−16086.
(41) Shvartsburg, A. A.; Jarrold, M. F. An Exact Hard-Spheres Scattering Model for the Mobilities of Polyatomic Ions. *Chem. Phys. Lett.* **1996**, *261*, 86−91.
(42) Knutson, E.; Whitby, K. Aerosol Classification by Electric Mobility: Apparatus, Theory, and Applications. *J. Aerosol Sci.* **1975**, *6*, 443−451.
(43) Maisser, A.; Barmpounis, K.; Holm, S.; Attoui, M.; Schmidt-Ott, A.; Kangasluoma, J.; Biskos, G. Characterization of Atmospheric-Pressure Spark Generated Atomic Silver and Gold Clusters by Time-Of-Flight Mass Spectrometry. *J. Aerosol Sci.* **2021**, *156*, 105780.
(44) Čížek, J. *Adv. Chem. Phys.* **1969**, 35−89, DOI: 10.1002/9780470143599.ch2.
(45) Bartlett, R J Many-Body Perturbation Theory and Coupled Cluster Theory for Electron Correlation in Molecules. *Annu. Rev. Phys. Chem.* **1981**, *32*, 359−401.
(46) Purvis, G. D.; Bartlett, R. J. A Full Coupled-Cluster Singles and Doubles Model: The Inclusion of Disconnected Triples. *J. Chem. Phys.* **1982**, *76*, 1910−1918.
(47) Watts, J. D.; Bartlett, R. J. Triple Excitations in Coupled-Cluster Theory: Energies and Analytical Derivatives. *Int. J. Quantum Chem.* **1993**, *48*, 51−66.
(48) Ramabhadran, R. O.; Raghavachari, K. Extrapolation to the Gold-Standard in Quantum Chemistry: Computationally Efficient and Accurate CCSD(T) Energies for Large Molecules Using an Automated Thermochemical Hierarchy. *J. Chem. Theory Comp.* **2013**, *9*, 3986−3994.
(49) Frisch, M. J.; Trucks, G. W.; Schlegel, H. B.; Scuseria, G. E.; Robb, M. A.; Cheeseman, J. R.; Scalmani, G.; Barone, V.; Petersson, G. A.; Nakatsuji, H.; et al. *Gaussian 16*, rev C.01; 2016.
(50) Zhang, J.; Dolg, M. ABCluster: The Artificial Bee Colony Algorithm for Cluster Global Optimization. *Phys. Chem. Chem. Phys.* **2015**, *17*, 24173−24181.
(51) Zhang, J.; Dolg, M. Global Optimization of Clusters of Rigid Molecules Using the Artificial Bee Colony Algorithm. *Phys. Chem. Chem. Phys.* **2016**, *18*, 3003−3010.
(52) Zhang, J.; Glezakou, V.-A.; Rousseau, R.; Nguyen, M.-T. NWPEsSe: An Adaptive-Learning Global Optimization Algorithm for Nanosized Cluster Systems. *J. Chem. Theory Comput.* **2020**, *16*, 3947−3958.
(53) Zhao, Y.; Truhlar, D. G. The M06 Suite of Density Functionals for Main Group Thermochemistry, Thermochemical Kinetics, Noncovalent Interactions, Excited States, and Transition Elements: Two New Functionals and Systematic Testing of Four M06-Class Functionals and 12 Other Function. *Theor. Chem. Acc.* **2008**, *120*, 215−241.
(54) Chen, M.; Dyer, J. E.; Li, K.; Dixon, D. A. Prediction of Structures and Atomization Energies of Small Silver Clusters, $(Ag)_n$, $n < 100$. *J. Phys. Chem. A* **2013**, *117*, 8298−8313.
(55) Dunning, T. H. Gaussian Basis Sets for Use in Correlated Molecular Calculations. I. The Atoms Boron through Neon and Hydrogen. *J. Chem. Phys.* **1989**, *90*, 1007−1023.
(56) Kendall, R. A.; Dunning, T. H.; Harrison, R. J. Electron Affinities of the First-Row Atoms Revisited. Systematic Basis Sets and Wave Functions. *J. Chem. Phys.* **1992**, *96*, 6796−6806.
(57) Peterson, K. A.; Puzzarini, C. Systematically Convergent Basis Sets for Transition Metals. II. Pseudopotential-Based Correlation Consistent Basis Sets For The Group 11 (Cu, Ag, Au) and 12 (Zn, Cd, Hg) Elements. *Theor. Chem. Acc.* **2005**, *114*, 283−296.
(58) Figgen, D.; Rauhut, G.; Dolg, M.; Stoll, H. Energy-Consistent Pseudopotentials for Group 11 And 12 Atoms: Adjustment to Multi-Configuration Dirac−Hartree−Fock Data. *Chem. Phys.* **2005**, *311*, 227−244.
(59) Von Helden, G.; Hsu, M. T.; Gotts, N.; Bowers, M. T. Carbon Cluster Cations with up to 84 Atoms: Structures, Formation Mechanism, and Reactivity. *J. Phys. Chem.* **1993**, *97*, 8182−8192.
(60) Mantina, M.; Chamberlin, A. C.; Valero, R.; Cramer, C. J.; Truhlar, D. G. Consistent van der Waals Radii for the Whole Main Group. *J. Phys. Chem. A* **2009**, *113*, 5806−5812.
(61) Campuzano, I.; Bush, M. F.; Robinson, C. V.; Beaumont, C.; Richardson, K.; Kim, H.; Kim, H. I. Structural Characterization of Drug-Like Compounds by Ion Mobility Mass Spectrometry: Comparison of Theoretical and Experimentally Derived Nitrogen Collision Cross Sections. *Anal. Chem.* **2012**, *84*, 1026−1033.
(62) Weis, P.; Welz, O.; Vollmer, E.; Kappes, M. M. Structures of Mixed Gold-Silver Cluster Cations $(Ag_mAu_n^+, m + n < 6)$: Ion Mobility Measurements and Density-Functional Calculations. *J. Chem. Phys.* **2004**, *120*, 677−684.
(63) Lindinger, W.; Albritton, D. L. Mobilities of Various Mass-Identified Positive Ions in Helium and Argon. *J. Chem. Phys.* **1975**, *62*, 3517−3522.
(64) Reed, A. E.; Weinstock, R. B.; Weinhold, F. Natural Population Analysis. *J. Chem. Phys.* **1985**, *83*, 735−746.
(65) Sannigrahi, A. B.; Nandi, P. K.; Schleyer, P. R. Ab Initio Theoretical Study of the Electronic Structure, Stability and Bonding of Dialkali Halide Cations. *Chem. Phys. Lett.* **1993**, *204*, 73−79.
(66) Gross, K. C.; Seybold, P. G. Substituent Effects on the Physical Properties and pK_a of Aniline. *Int. J. Quantum Chem.* **2000**, *80*, 1107−1115.
(67) Huber, K. P.; Herzberg, G. In *Molecular Spectra and Molecular Structure*; Springer, 1979. DOI: 10.1007/978-1-4757-0961-2_2.
(68) Schmidt, M.; Masson, A.; Cheng, H.-P.; Bréchignac, C. Physisorption and Chemisorption on Silver Clusters. *ChemPhysChem* **2015**, *16*, 855−865.
(69) Larriba-Andaluz, C.; Carbone, F. The Size-Mobility Relationship of Ions, Aerosols, and Other Charged Particle Matter. *J. Aerosol Sci.* **2021**, *151*, 105659.
(70) Ku, B. K.; de la Mora, J. F. Relation between Electrical Mobility, Mass, and Size for Nanodrops 1−6.5 nm in Diameter in Air. *Aerosol Sci. Technol.* **2009**, *43*, 241−249.
(71) Thomas, J. M.; He, S.; Larriba-Andaluz, C.; DePalma, J. W.; Johnston, M. V.; Hogan, C. J., Jr. Ion Mobility Spectrometry-Mass Spectrometry Examination of the Structures, Stabilities, and Extents of Hydration of Dimethylamine−Sulfuric Acid Clusters. *Phys. Chem. Chem. Phys.* **2016**, *18*, 22962−22972.
(72) Herley, P. J.; Prout, E. G. The Thermal Decomposition of Silver Oxide. *J. Am. Chem. Soc.* **1960**, *82*, 1540−1543.

https://doi.org/10.1021/acs.jpca.2c02809
J. Phys. Chem. A 2022, 126, 6376−6386